Hindawi
Journal of Chemistry
Volume 2021, Article ID 3762917, 9 pages
https://doi.org/10.1155/2021/3762917

Research Article

Novel One-Pot Solvothermal Synthesis of High-Performance Copper Hexacyanoferrate for Cs^+ Removal from Wastewater

Chi Ma,[1] Zhenzhen Jiang,[1,2] Senjian Han ,[1] Yafei Guo,[1] and Tianlong Deng [1]

[1]*Key Laboratory of Marine Resource Chemistry and Food Technology (TUST), Ministry of Education, Tianjin Key Laboratory of Brine Chemical Engineering and Resource Eco-Utilization, College of Marine and Environmental Science, Tianjin University of Science and Technology, Tianjin 300457, China*
[2]*Central Laboratory of Tibet Autonomous Region Bureau of Geological & Mineral Resources, Lhasa 850033, China*

Correspondence should be addressed to Senjian Han; senjhan@tust.edu.cn and Tianlong Deng; tldeng@tust.edu.cn

Received 13 August 2021; Revised 8 September 2021; Accepted 11 September 2021; Published 23 September 2021

Academic Editor: Gang Feng

Efficient removal of radioactive cesium from complex wastewater is a challenge. Unlike traditional precipitation and hydrothermal synthesis, a novel vast specific surface area adsorbent of copper hexacyanoferrates named EA-CuHCF was synthesized using a one-pot solvothermal method under the moderate ethanol media characterized by XRD, SEM, EDS, BET, and FTIR. It was found that the maximum adsorption capacity towards Cs^+ was 452.5 mg/g, which is far higher than most of the reported Prussian blue analogues so far. Moreover, EA-CuHCF could effectively adsorb Cs^+ at a wide pH range and low concentration of Cs^+ in geothermal water within 30 minutes, and the removal rate of Cs^+ was 92.1%. Finally, the separation factors between Cs^+ and other competitive ions were higher than 553, and the distribution coefficient of Cs^+ reached up to 2.343×10^4 mL/g. These properties suggest that EA-CuHCF synthesized by the solvothermal method has high capacity and selectivity and can be used as a candidate for Cs^+ removal from wastewater.

1. Introduction

Nuclear power plays a significant role in transitioning the energy supply [1]. However, the accidental leakage of the nuclear power plant could cause considerable harm to humans [2–4]. ^{137}Cs is one of the most dangerous isotopes. Its long half-life, high energy β/γ emission, and high solubility could make its way into the human body, leading to an increased incidence of cancer, leukemia, and genetic diseases [5–10]. For example, the Chernobyl accident in 1986 and the Fukushima accident in 2011 led to the accidental release of large amounts of ^{137}Cs [9, 10]. As a result, the surrounding regions and waters have been seriously polluted. From environmental restoration and human health, it is essential and urgent to remove radioactive cesium from wastewater efficiently [11–15].

Adsorption is one of the most concerning methods for cesium removal, particularly suitable for the separation at trace levels. It is an effective technique for large-scale and efficient cesium separation due to its high adsorption efficiency, low cost, easy operation, and negligible secondary pollution [16–19]. To date, a variety of adsorbents have been developed, such as clay minerals, ammonium molybdophosphate, metal sulfides, and metal hexacyanoferrates (MHCFs) [20–25]. Among them, MHCFs, also known as Prussian blue (PB) or Prussian blue analogues (PBAs), presented superior selectivity and adsorption capacity due to their unique cesium affinity [13, 26–32]. Moreover, this family of compounds is low cost, chemically stable, and low toxicity, so they have been extensively investigated. However, the limited direct use of MHCFs made it attractive to immobilize MHCFs onto substrate materials, which severely reduced cesium adsorption capacity. Therefore, a variety of approaches have been taken into account to maximize the performance of MHCFs, mainly focusing on the immobilization form or structure of composites [33–37]. An outstanding MHCF could also make a breakthrough in the adsorption performance of composite adsorbents.

Generally, the precipitation method is used to synthesize MHCFs of targeted size or structure based on mixing of M^{n+} and $[M'(CN)_6]^{m-}$ by adding a protective agent or controlling the precursor concentration as well as the addition rate [38–40]. However, the overquick reaction rate of the precursors may cause the obtained MHCFs to be compact and aggregated, which are adverse to sufficiently exposing active sites and accessibly reacting with Cs^+. To date, solvothermal and hydrothermal methods have been explored to improve Cs^+ adsorption capacity by effectively constructing different structures, morphologies, and sizes of PBAs with high surface areas [41–43]. For example, the hydrothermal method has been applied to inhibit PB aggregation with ordered hollow structures, improving the maximum adsorption capacity from 29.3 mg/g to 262 mg/g. It can be explained that the hollow structure of PB ($S_{BET} = 338\ m^2/g$) provided more channels for Cs^+ penetration and adsorption. In comparison, the commercial PB ($S_{BET} = 84\ m^2/g$) with aggregated fine nanoparticles might only adsorb Cs^+ on the external surface [42]. Similarly, a hierarchical PB composed of ultrathin nanosheets (HPBN, $S_{BET} = 246\ m^2/g$) was prepared by the solvothermal method with improved Cs^+ uptakes of 200 mg/g because of exposure micropores of the rearranged structure [43]. Therefore, it is reasonable to assume that changing solvent or reaction temperature could alter the reaction process. To the best of our knowledge, it has been studied scarcely on synthesizing nanostructured adsorbents with high surface areas except for PB (FeHCF), eventhough PB shows the lowest capacity among the MHCFs.

In this study, the solvothermal method was experimentally studied to synthesize porous CuHCF for cesium removal. As excepted, the results of adsorption capacity indicate that all the tested factors (solvent, reaction temperature, and precursor ratios) impact the adsorption performance of CuHCF, and the optimal conditions were selected for fabricating targeted EA-CuHCF. Furthermore, the effects of pH, contact time, temperature, competitive ions, and initial concentration on the adsorption performance were investigated systematically, while XRD, SEM, FTIR, and BET were conducted to reveal the structure and surface properties. The results indicated EA-CuHCF could be considered as a promising candidate for ^{137}Cs removal from wastewater.

2. Experimental

2.1. Materials. It is of particular concern to avoid the harmful effects of radioactive cesium (^{137}Cs). Therefore, nonradioactive cesium (^{133}Cs) with similar chemical and physical properties was used. CsCl, $K_3[Fe(CN)_6]$ and $CuCl_2{\cdot}3H_2O$ were purchased from J&K Scientific Ltd. Methanol, ethanol, and ethylene glycol were brought from Sinopharm Chemical Reagent Co., Ltd. Geothermal water was sampled from a bore well in the Tibet autonomous region. The stock Cs^+ solution of 100 mg/L was prepared by dissolving 0.1267 g CsCl in 1000 mL deionized water, and a specific concentration of Cs solution was obtained by quantitative dilution. All reagents used in the experiment were analytical grade without further purification.

2.2. Synthesis of CuHCF. CuHCF was synthesized by the solvothermal method under various conditions. In a typical experiment, 2.0 mmol $CuCl_2$, 0.5 mmol $K_3Fe(CN)_6$, and 20 mL ethanol (EA) were added into a 50.0 mL hydrothermal kettle. Then, the hydrothermal kettle was put into an oven at 100°C for 24 h. After centrifugation, the product was washed thoroughly with anhydrous ethanol and deionized water. After drying, the desired CuHCF was obtained, named EA-CuHCF. The synthesis procedure is shown in Figure 1. On this basis, solvent (methanol (MA), ethanol (EA), and ethylene glycol (EG)), reaction temperature (80, 100, and 120°C), and precursor ratios ($CuCl_2$: $K_3Fe(CN)_6$ = 1 : 2, 1 : 1, 2 : 1, 3 : 1, 4 : 1, 5 : 1, and 6 : 1) were changed successively to synthesize different CuHCF, testing adsorption capacity as the criteria.

2.3. Characterization. ICP-OES (VISTA MPX, USA) was used to determine the concentrations of cesium ions in the solutions before and after adsorption. Scanning electron microscopy (SEM, JSM-IT300LV, Japan) was conducted to observe the surface morphologies of EA-CuHCF before and after adsorption. Powder X-ray diffraction (XRD) was collected on an X-ray diffractometer using Cu Kα radiation over a 2θ range of 5–75° and X-ray power of 36 kV/20 mA at a scan (MSAL XD-3, Beijing Purkinje General Instrument Co., Ltd., China). The BET surface area was measured by an Auto-sorb-iQA3200-4 (Quantatech Co.). FTIR spectra were performed in the range of 4000–400 cm^{-1} with an accumulation of 16 scans (Tensor27, Germany).

2.4. Adsorption Experiments. Batch experiments were conducted to estimate the adsorption performance of the developed adsorbents for Cs^+. The adsorption capacity (q_e, mg/g), removal rate (R, %) distribution coefficient (K_d, mL/g), and separation factor (α_{Me}^{Cs}) were calculated according to the following formulas [4].

$$q_e = \frac{(c_0 - c_e) \times V}{m}, \tag{1}$$

$$R = \frac{c_0 - c_e}{c_0} \times 100\%, \tag{2}$$

$$K_d = \frac{c_0 - c_e}{c_e} \times \frac{V}{m}, \tag{3}$$

$$\alpha_{Me}^{Cs} = \frac{K_d\,(Cs)}{K_d\,(Me)}, \tag{4}$$

where c_0 (mg/L) is the initial concentration, c_e (mg/L) is the equilibrium concentration, V (mL) is the volume of the solution, m (g) is the weight of the adsorbent, and Me represents the other alkali metal ions.

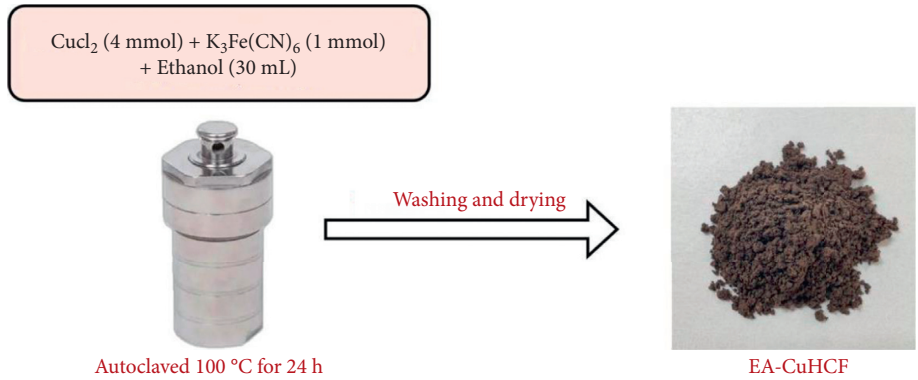

Figure 1: Diagram of the process of solvothermal synthesis of EA-CuHCF.

2.4.1. Effect of pH. The effect of pH on the adsorption performance was investigated by adjusting pH values of Cs solutions from 2 to 10 with 0.1 mol/L NaOH and 0.1 mol/L HCl. In an experiment, 0.05 g CuHCF and 100 mL of 100 mg/L CsCl solution were successively added into a 250 mL beaker and then stirred on a magnetic stirrer for 30 min. After adsorption, the Cs^+ concentration of the residual solution was determined.

2.4.2. Effect of Competing Ions. In order to find out the selectivity of CuHCF, the influence of competitive ions on the adsorption performance was investigated, using geothermal water as the complex system containing high concentrations of various ions. 0.05 g CuHCF and 100 mL of geothermal water were added into a 250 mL beaker and then stirred on a magnetic stirrer for 30 min. The adsorption experiment was carried out at room temperature and natural pH.

2.4.3. Adsorption Kinetics. Adsorption kinetics was determined by studying the effect of contact time on Cs^+ adsorption. 0.05 g CuHCF and 100 mL of 100 mg/L CsCl solution were mixed and stirred at room temperature in natural pH. Samples were taken at 15, 30, 60, 120, 180, 240, and 600 min, respectively.

In order to evaluate the kinetic mechanism of Cs^+ adsorption on CuHCF, the most commonly used models of pseudo-first-order and pseudo-second-order equations are introduced to analyze the experimental data. The equations are expressed as follows [40]:

$$q_t = q_e \times \left(1 - e^{-k_1 t}\right),$$
$$q_t = \frac{q_e^2 k_2 t}{1 + q_e k_2 t}, \tag{5}$$

where q_e and q_t are the adsorption capacities (mg/g) of CuHCF for Cs^+ at equilibrium and a specific time t (min), respectively. K_1 (min^{-1}) and K_2 ($g \cdot mg^{-1} \cdot min^{-1}$) are the rate constants of pseudo-first-order and pseudo-second-order equation models.

2.4.4. Adsorption Isotherm. Adsorption isotherm was tested by changing the initial concentrations of Cs^+ solution (60, 150, 250, 650, and 1300 mg/L). 0.05 g CuHCF was added to 100 mL CsCl solutions with different concentrations of Cs^+, and a series of adsorption experiments were studied for 30 min at room temperature and natural pH.

In order to further study the adsorption characterization of Cs^+ by CuHCF, two isothermal models, namely, linear Langmuir and Freundlich adsorption models, were used to analyze the adsorption data. The equations are expressed as follows [7]:

$$\frac{c_e}{q_e} = \frac{1}{q_e \times K_L} + \frac{c_e}{q_m},$$
$$q_e = K_F C_e^{1/n}, \tag{6}$$
$$\ln q_e = \ln K_F + \frac{\ln c_e}{n},$$

where q_e (mg/g) and c_e (mg/L) are the equilibrium quantities of adsorption capacity and concentration, respectively, q_m (mg/g) is the maximum adsorption capacity, K_L (L/mg) and K_F (mg/g) are the constants of Langmuir and Freundlich isotherms, and n is related to adsorption strength.

3. Results and Discussion

3.1. Optimization of Reaction Conditions. The synthesis of CuHCF under different reaction solvents, such as methanol, ethanol, and ethylene glycol, was studied. The influence of varying reaction solvents on Cs^+ adsorption capacity is shown in Figure 2(a). It was found that the tested solvents affected adsorption performance inconspicuously, and the most significant disparity was only 9.0%. When considering the cost and low toxicity of solvents, ethanol was selected as the reaction solvent for further study.

Different reaction temperatures of 80, 100, and 120°C were then investigated, respectively, and the capacities are shown in Figure 2(b). Similarly, the tested temperatures had little influence on adsorption capacity, and generally, the materials synthesized at higher temperatures presented relatively better adsorption performance. So, the reaction temperature was determined to be 100°C.

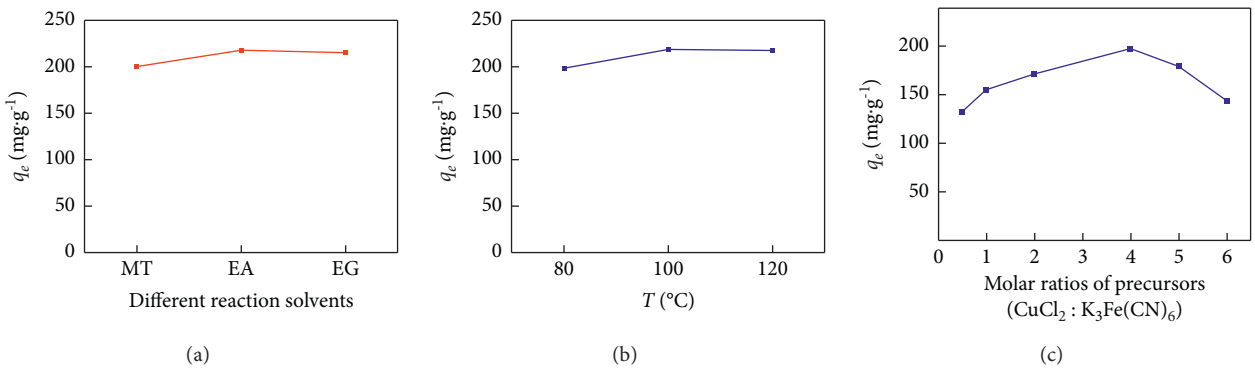

Figure 2: Effects of different reaction conditions on adsorption capacity: (a) solvents, (b) reaction temperatures, and (c) molar ratios of precursor ($c_0 = 110$ mg/L, $m/V = 0.5$ g/L, $T = 298$ K).

Finally, different ratios of precursors were investigated, and the results are plotted in Figure 2(c). It can be seen that with the increased molar ratio of $CuCl_2$ to $K_3Fe(CN)_6$, the Cs^+ adsorption capacity first increases and then decreases. The molar ratio of precursors 4 : 1 ($CuCl_2$: $K_3Fe(CN)_6 = 4:1$) demonstrated the maximum Cs^+ adsorption capacity. As mentioned above, the optimum conditions of the solvothermal method fabricating CuHCF have controlled precursor ratios of 4 : 1 at 100°C using ethanol as a solvent in the following experiments. The satisfying material was named EA-CuHCF.

3.2. Characterization. SEM analyzed the obtained EA-CuHCF with maximum adsorption capacity, and the images are shown in Figures 3(a) and 3(b). It can be seen that the EA-CuHCF has a typical cubic structure. Moreover, EA-CuHCF is nanosized, and the particle size distribution of EA-CuHCF is narrow. All the morphologies observed contribute to improving the adsorption capacity positively. Furthermore, the surface morphology of EA-CuHCF after adsorption is also displayed, which does not change visibly compared with that of before adsorption, indicating high stability.

The crystal phase and structure of EA-CuHCF ($CuCl_2$: $K_3Fe(CN)_6 = 4:1$) was identified by X-ray diffraction (XRD), and the XRD pattern is shown in Figure 4(a). The diffraction peaks of $2\theta = 17.4°$, 24.7°, 35.2°, 39.6°, 43.5°, 50.7°, 54.1°, and 57.2° were attributed to crystalline planes (200), (220), (400), (420), (422), (440), (422), and (620) of CuHCF (JCPDS file no. 86–513). The XRD pattern of the as-prepared EA-CuHCF was in excellent agreement with the previously reported in the literature [44].

To gain more information on structure, EA-CuHCF was characterized by FTIR measurements. As shown in Figure 4(b), the attached FTIR spectra of EA-CuHCF are illustrated in the range of 400–4000 cm^{-1}. The peaks at 595 cm^{-1} are consistent with C-N stretching in Fe^{III}-CN-Cu^{II}, and the peaks near 2098 cm^{-1} are related to the tensile vibration absorption band of the group -C≡N [44]. Moreover, the main peaks remain unchanged after adsorbed Cs^+. All the aforementioned characterizations of EA-CuHCF confirmed the successful synthesis.

N_2 sorption measurement at 77 K discloses a Brunauer–Emmett–Teller (BET) surface area of 325 m^2/g for EA-CuHCF, indicating the presence of inherent micropores. Moreover, the pore size distribution curve (Figure 5(b)) calculated from the desorption process by the Barrett–Joynes–Halenda (BJH) method reveals the average pore size of 3.6 nm. It is noted that the hydrated cesium ionic radius is 0.33 nm. The large specific surface area and porous structure are compelling evidence for the high adsorption performance of EA-CuHCF.

3.3. Effect of pH Value on Adsorption. The effect of pH on Cs^+ adsorption was conducted at various pH values with an initial Cs^+ concentration of 100 mg/L and a liquid-solid ratio of 2000 : 1. As the results are shown in Figure 6(a), the adsorption capacities of EA-CuHCF remained at a high level over a wide pH, indicating that it has a more negligible effect on pH. So, it is believed that EA-CuHCF could be used in Cs removal from diversified aqueous solutions. For convenience, the subsequent experiments were carried out in a natural pH environment.

3.4. Effects of Competing Ions on Adsorption. The adsorption of Cs^+ could be hindered by other coexisted alkali metal ions [30]. In order to evaluate the selectivity of EA-CuHCF, the experiments were carried out using geothermal water in the presence of high concentrations of Na^+, K^+, and Li^+. The relevant parameters of the main interfering ions in geothermal water are presented in Table 1. According to the concentrations before and after adsorption, the adsorption efficiency of Cs^+ was calculated to be 92.1%, while those for Na^+, K^+, and Li^+ were negligible. It was worth saying the concentration of K^+ was higher than that in initial geothermal water, which could be attributed to the ion exchange between K^+ and Cs^+, and the molar ratio of the released K^+ to adsorbed Cs^+ was approximately 1. Besides, it is observed that distribution coefficients (K_d) are as high as 2.343×10^4 mL/g for Cs^+ and separation factors (α_{Me}^{Cs}) are in high levels, meaning that EA-CuHCF has favorable adsorption selectivity for cesium ions. From this point of view, EA-CuHCF can be a suitable adsorbent for Cs^+ even in complex solutions.

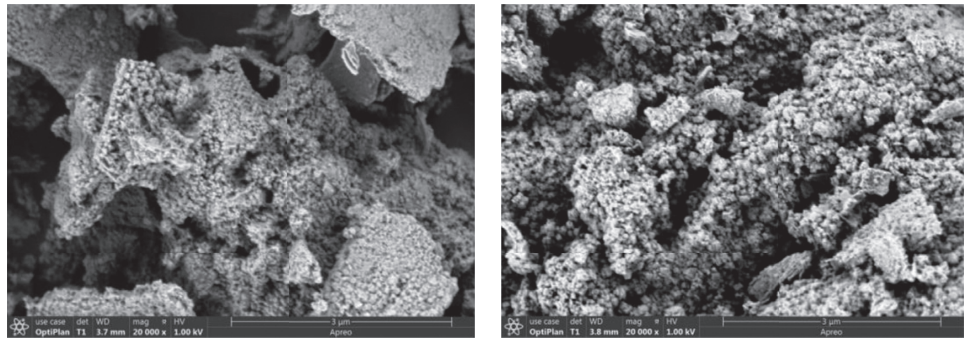

(a) (b)

Figure 3: SEM images of EA-CuHCF before (a) and after (b) adsorption.

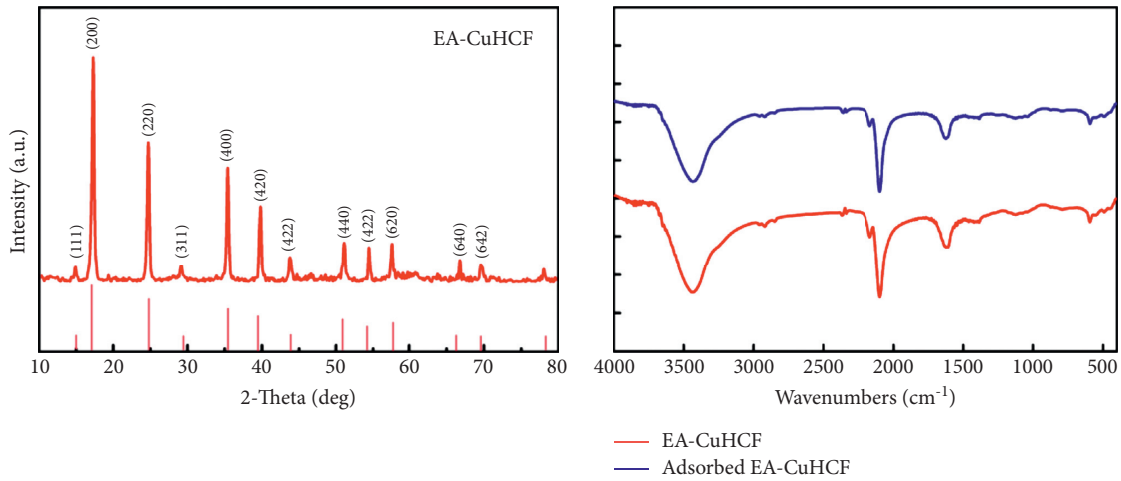

(a) (b)

Figure 4: X-ray diffraction patterns of EA-CuHCF (a) and FTIR spectra of EA-CuHCF before and after adsorption (b).

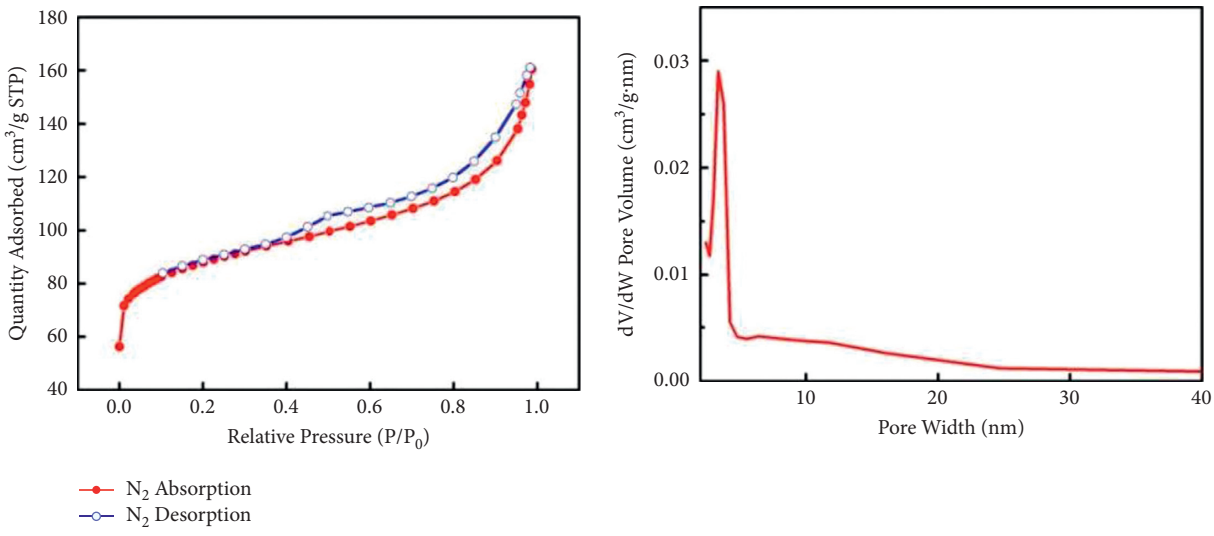

(a) (b)

Figure 5: N_2 adsorption-desorption isotherms (a) and corresponding BJH pore size distribution curve (b) of EA-CuHCF.

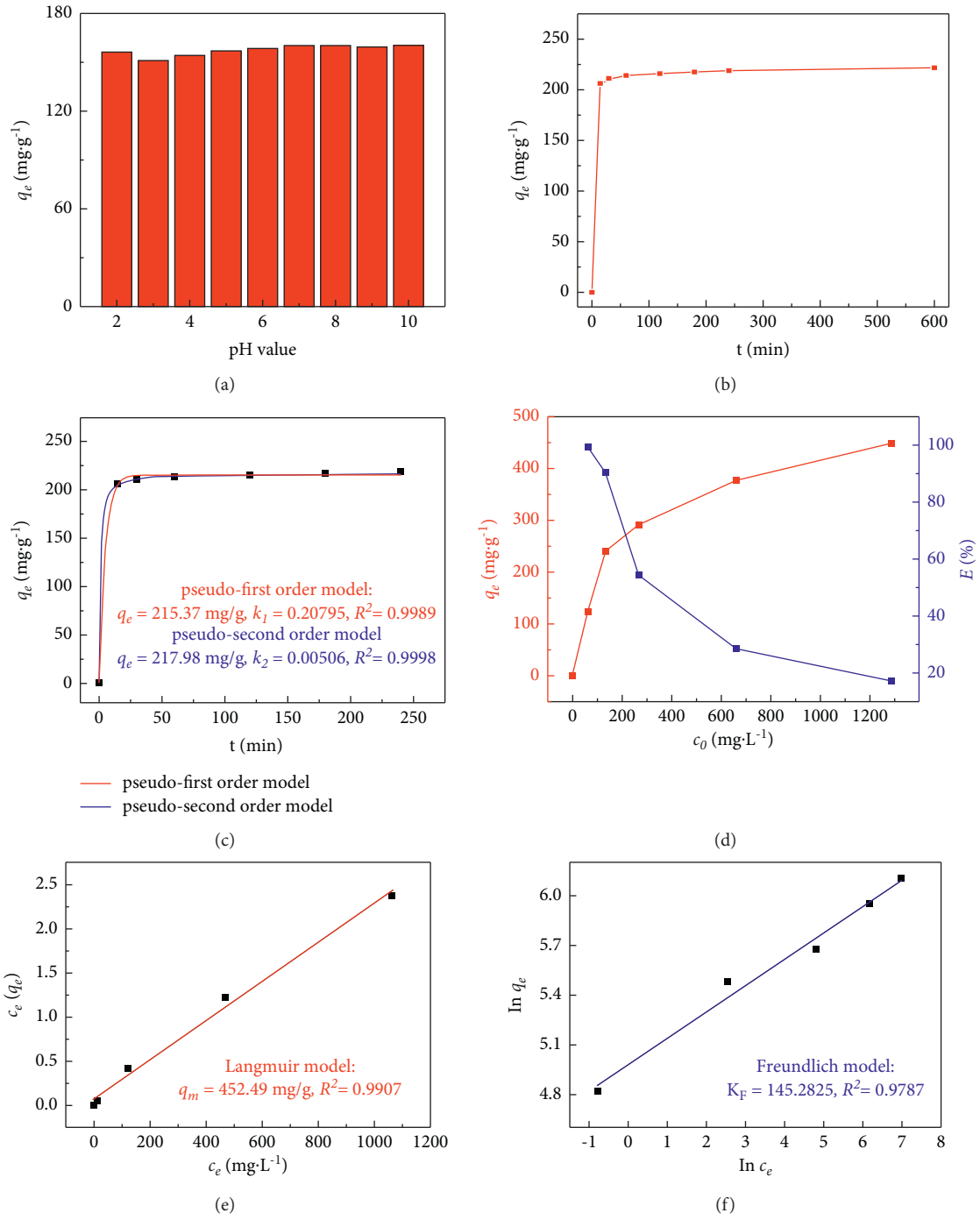

Figure 6: Effect of pH value on adsorption capacity (a). Influence of contact time on Cs^+ adsorption (b). Nonlinear fitting diagrams of the adsorption kinetic model (c) (c_0 = 110 mg/L, m/V = 0.5 g/L, T = 298 K). Effects of initial concentration on Cs^+ adsorption (d). Linear fitting diagram of Langmuir (e) and Freundlich (f) isotherm models (c_0 = 60–1300 mg/L, m/V = 0.5 g/L, t = 0.5 h).

Table 1: The selectivity parameters of Cs^+ against the coexisted ions.

	Na	K	Li	Cs
c_0 (mg/L)	720.02	169.44	24.62	14.62
c_e (mg/L)	715.93	173.03	24.11	1.15
R (%)	0.59	—	2.07	92.10
K_d (mL/g)	11.43	—	42.31	2.34×10^4
α_{Me}^{Cs}	2050.30	—	553.73	1.00

—, not available.

3.5. Effect of Contact Time and Adsorption Kinetics. As a function of contact time, the EA-CuHCF adsorption capacity is presented in Figure 6(b). Accordingly, the adsorption capacity of EA-CuHCF increased rapidly within the beginning 15 min and reached a maximum within 30 min, achieving adsorption equilibrium. The rapid adsorption rate might be attributed to the existing numerous active sites of the adsorbent in the initial stage, in which Cs^+ is occupied with the ongoing adsorption process, and the adsorption equilibrium is reached.

Table 2: Summary of the adsorption capacity of various Prussian blue adsorbents.

Adsorbent	Synthetic method	S_{BET} (m^2/g)	q_{max} (mg/g)	Ref.
GP-CuHCF	Precipitation	—	328	[33]
CuHCF-carbomer	Precipitation	—	230.1	[34]
PBA@ZnTi LDH	Precipitation	—	243.9	[35]
Hollow PB nanoparticles	Hydrothermal	338	262	[42]
HPBN	Solvent-thermal	246	200	[43]
PB/Fe_3O_4	Precipitation	322.19	280.8	[45]
MOF/KNiFC	Solvent-thermal	47.74	153	[46]
MOF/Fe_3O_4/KNiFC	Solvent-thermal	111.7	109.1	[46]
Bulk CuHCF	Precipitation	—	251.4	[47]
hf-TifC	Precipitation (sacrificial template)	63.89	454.54	[48]
EA-CuHCF	Solvent-thermal	350	452.5	This work

[a]Not mentioned.

Further investigation was conducted by fitting the pseudo-first-order model and pseudo-second-order model to adsorption kinetic data. As shown in Figure 6(c), the higher correlation coefficient ($R^2 = 0.9998$) suggests that the pseudo-second-order model is more suitable than the pseudo-first-order model ($R^2 = 0.9989$), indicating chemical adsorption played a considerable role. Therefore, combing the molar ratio of released K^+ to adsorbed Cs^+, ion exchange is the most probable adsorption mechanism.

3.6. Effect of Cs^+ Concentration and Adsorption Isotherm. Effects of initial Cs^+ concentration on the adsorption process are shown in Figure 6(d). Typically, Cs^+ adsorption capacity increased sharply when the initial concentration was less than 150 mg/L, then raised slowly, and reached 450 mg/g with the initial concentration increased to 1300 mg/L. The rapidly increased adsorption capacity was owed to the great accessible Cs^+ adsorption sites and increased initial concentration leading to a high driving force for mass transfer. In contrast, the slightly increased adsorption capacity was attributed to the available adsorption sites tending to be occupied, confirmed by the decreased removal rate. Briefly, EA-CuHCF can effectively adsorb Cs^+ in a wide initial concentration range, especially in low concentrations, further demonstrating its possible application in Cs^+ removal from wastewater of low concentration.

Adsorption isotherm on Cs^+ adsorption was fitted to clarify the adsorption mechanism with nonlinear Langmuir and Freundlich isotherm models, and the results are shown in Figures 6(e) and 6(f), respectively. The higher correlation coefficient ($R^2 = 0.9789$) demonstrates that the adsorption is more likely to follow the Langmuir model, suggesting monolayer adsorption formed on the surface of absorbent uniformly, without interacting with each other, calculated maximum adsorption capacity is 452.5 mg/g.

3.7. Comparison with Other Adsorbents of Prussian Blue Analogues. When compared EA-CuHCF with other PBA adsorbents, the maximum uptakes of some previously reported PBAs as well as their composites, such as hollow PB nanoparticles, hf-TiFC, and bulk CuHCF, are summarized in Table 2. Meanwhile, the BET surface area and synthetic method are also presented. As given in Table 2, the adsorption capacity of EA-CuHCF was much higher than most of the reported materials, including substrate-loaded PBAs, such as PB/Fe_3O_4 (280.82 mg/g) [45] and MOF/KNiFC (155 mg/g) [46], and different kinds of PBAs, such as hollow PB nanoparticles (262 mg/g) [42] and bulk CuHCF (251.4, coprecipitation) [46]. Therefore, it is believed that solvothermal is an effective way to synthesize EA-CuHCF with excellent potential to remove Cs^+ from contaminated outflows.

4. Conclusion

In this study, it is the first time to synthesize a crystalline porous adsorbent EA-CuHCF by the solvothermal method for Cs^+ removal. Adsorption isotherm results indicated the maximum adsorption capacity reached up to 452.5 mg/g, which was much higher than most reported PBA absorbents. Moreover, kinetics results suggested that the adsorption equilibrium could be reached within 30 min, and the adsorption was more likely to be ion exchange. At the same time, EA-CuHCF material had excellent selectivity to Cs^+ according to the results obtained in geothermal water. We believe that EA-CuHCF has tremendous potential for Cs^+ removal in wastewater.

Data Availability

The data used to support the findings of this study are available from the corresponding author upon request.

Conflicts of Interest

The authors declare that they have no conflicts of interest.

Acknowledgments

The authors gratefully acknowledge partial financial supports from the National Natural Science Foundation of China (22073068), Tianjin Key Laboratory of Brine Chemical Engineering and Resource Eco-Utilization (BCERE201905), and the Yangtze Scholars and Innovative Research Team of the Chinese University (IRT_17R81).

References

[1] V. D. M. Anton, "Nuclear energy saves lives," *Nature*, vol. 570, p. 33, 2019.

[2] S. Yang, C. Han, X. Wang, and M. Nagatsu, "Characteristics of cesium ion sorption from aqueous solution on bentonite-and carbon nanotube-based composites," *Journal of Hazardous Materials*, vol. 274, pp. 46–52, 2014.

[3] M. Miyazaki, K. Tanigawa, and M. Murakami, "After Fukushima: creating a dialogue," *Science*, vol. 352, no. 6286, p. 666, 2016.

[4] S. Q. Chen, J. Y. Hu, G. L. Mi, Y. F. Guo, and T. L. Deng, "Novel montmorillonite-sulfur composite for enhancement of selective adsorption toward cesium," *Green Energy & Environment*, 2020.

[5] D. Alby, C. Charnay, M. Heran, B. Prelot, and J. Zajac, "Recent developments in nanostructured inorganic materials for sorption of cesium and strontium: synthesis and shaping, sorption capacity, mechanisms, and selectivity-a review," *Journal of Hazardous Materials*, vol. 344, pp. 511–530, 2018.

[6] H. Long, P. Wu, and N. Zhu, "Evaluation of Cs^+ removal from aqueous solution by adsorption on ethylamine-modified montmorillonite," *Chemical Engineering Journal*, vol. 225, pp. 237–244, 2013.

[7] S. Chen, J. Hu, J. Shi et al., "Composite hydrogel particles encapsulated ammonium molybdophosphate for efficiently cesium selective removal and enrichment from wastewater," *Journal of Hazardous Materials*, vol. 371, pp. 694–704, 2019.

[8] M.-L. Feng, D. Sarma, Y.-J. Gao et al., "Efficient removal of $[UO2]^{2+}$, Cs^+, and Sr^{2+} ions by radiation-resistant gallium thioantimonates," *Journal of the American Chemical Society*, vol. 140, no. 35, pp. 11133–11140, 2018.

[9] M. Hu, S. Furukawa, R. Ohtani et al., "Synthesis of Prussian blue nanoparticles with a hollow interior by controlled chemical etching," *Angewandte Chemie*, vol. 51, pp. 984–988, 2012.

[10] S. Sarina, A. Bo, D. Liu et al., "Separate or simultaneous removal of radioactive cations and anions from water by layered sodium vanadate-based sorbents," *Chemistry of Materials*, vol. 26, no. 16, pp. 4788–4795, 2014.

[11] T. Mizuno and H. Kubo, "Overview of active cesium contamination of freshwater fish in Fukushima and Eastern Japan," *Scientific Reports*, vol. 3, no. 1, p. 1742, 2013.

[12] D. Yang, S. Sarina, H. Zhu et al., "Capture of radioactive cesium and iodide ions from water by using titanate nanofibers and nanotubes," *Angewandte Chemie International Edition*, vol. 50, no. 45, pp. 10594–10598, 2011.

[13] J. Wang and S. Zhuang, "Removal of cesium ions from aqueous solutions using various separation technologies," *Reviews in Environmental Science and Bio/Technology*, vol. 18, no. 2, pp. 231–269, 2019.

[14] J. Lehto, R. Koivula, H. Leinonen, E. Tusa, and R. Harjula, "Removal of radionuclides from Fukushima Daiichi waste effluents," *Separation & Purification Reviews*, vol. 48, no. 2, pp. 122–142, 2019.

[15] S. Schmid, "Chernobyl: data wars and disaster politics," *Nature*, vol. 566, no. 7745, pp. 450-451, 2019.

[16] M. Castrillejo, N. Casacuberta, C. F. Breier, S. M. Pike, P. Masqué, and K. O. Buesseler, "Reassessment of ^{90}Sr, ^{137}Cs, and ^{134}Cs in the coast off Japan derived from the Fukushima dai-ichi nuclear accident," *Environmental Science & Technology*, vol. 50, no. 1, pp. 173–180, 2016.

[17] J. Zhang, L. Yang, T. Dong, F. Pan, H. Xing, and H. Liu, "Kinetics-controlled separation intensification for cesium and rubidium isolation from salt lake brine," *Industrial & Engineering Chemistry Research*, vol. 57, no. 12, pp. 4399–4406, 2018.

[18] S. Hao, Y. Geng, and Z. Jia, "UV pre-activation/thermal initiated grafting of caffeic acid on PVDF for preparation of adsorptive membranes for cesium," *Reactive and Functional Polymers*, vol. 132, pp. 120–126, 2018.

[19] T. Fujisaki, K. Kashima, M. Hagiri, and M. Imai, "Isothermal adsorption behavior of cesium ions in a novel chitosan-Prussian blue-based membrane," *Chemical Engineering & Technology*, vol. 42, no. 4, pp. 910–917, 2019.

[20] T. Wen, Z. Zhao, C. Shen et al., "Multifunctional flexible free-standing titanate nanobelt membranes as efficient sorbents for the removal of radioactive $^{90}Sr^{2+}$ and $^{137}Cs^+$ ions and oils," *Scientific Reports*, vol. 6, no. 1, p. 20920, 2016.

[21] J. Wang, S. Zhuang, and Y. Liu, "Metal hexacyanoferrates-based adsorbents for cesium removal," *Coordination Chemistry Reviews*, vol. 374, pp. 430–438, 2018.

[22] M.-L. Feng, D.-N. Kong, Z.-L. Xie, and X.-Y. Huang, "Three-dimensional chiral microporous germanium antimony sulfide with ion-exchange properties," *Angewandte Chemie International Edition*, vol. 47, no. 45, pp. 8623–8626, 2008.

[23] D. Ding, Y. Zhao, S. Yang et al., "Adsorption of cesium from aqueous solution using agricultural residue—walnut shell: equilibrium, kinetic and thermodynamic modeling studies," *Water Research*, vol. 47, no. 7, pp. 2563–2571, 2013.

[24] A. J. Celestian, J. D. Kubicki, J. Hanson, A. Clearfield, and J. B. Parise, "The mechanism responsible for extraordinary Cs ion selectivity in crystalline silicotitanate," *Journal of the American Chemical Society*, vol. 130, no. 35, pp. 11689–11694, 2008.

[25] A. Dyer, M. Pillinger, R. Harjula, and S. Amin, "Sorption characteristics of radionuclides on synthetic birnessite-type layered manganese oxides," *Journal of Materials Chemistry*, vol. 10, no. 8, pp. 1867–1874, 2000.

[26] R. Chen, H. Tanaka, T. Kawamoto et al., "Selective removal of cesium ions from wastewater using copper hexacyanoferrate nanofilms in an electrochemical system," *Electrochimica Acta*, vol. 87, pp. 119–125, 2013.

[27] M. A. Lilga, R. J. Orth, J. P. H. Sukamto, S. M. Haight, and D. T. Schwartz, "Metal ion separations using electrically switched ion exchange," *Separation and Purification Technology*, vol. 11, no. 3, pp. 147–158, 1997.

[28] A. K. Vipin, B. Hu, and B. Fugetsu, "Prussian blue caged in alginate/calcium beads as adsorbents for removal of cesium ions from contaminated water," *Journal of Hazardous Materials*, vol. 258-259, pp. 93–101, 2013.

[29] X. Long, R. Chen, J. Tan, Y. Lu, and Q. Lei, "Electrochemical recovery of cobalt using nanoparticles film of copper hexacyanoferrates from aqueous solution," *Journal of Hazardous Materials*, vol. 384, Article ID 121252, 2019.

[30] Q. Tao, X. Zhang, D. Huang et al., "Copper hexacyanoferrate nanoparticle-decorated biochar produced from pomelo peel for cesium removal from aqueous solution," *Journal of Radioanalytical and Nuclear Chemistry*, vol. 322, no. 2, pp. 791–799, 2019.

[31] H. Kim, M. Kim, W. Kim, W. Lee, and S. Kim, "Photocatalytic enhancement of cesium removal by Prussian blue-deposited TiO_2," *Journal of Hazardous Materials*, vol. 357, pp. 449–456, 2018.

[32] Y. Zheng, J. Qiao, J. Yuan, J. Shen, A.-J. Wang, and L. Niu, "Electrochemical removal of radioactive cesium from nuclear waste using the dendritic copper hexacyanoferrate/carbon nanotube hybrids," *Electrochimica Acta*, vol. 257, pp. 172–180, 2017.

[33] R. Turgis, G. Arrachart, C. Delchet et al., "An original "click and bind" approach for immobilizing copper hexacyanoferrate nanoparticles on mesoporous silica," *Chemistry of Materials*, vol. 25, no. 21, pp. 4447–4453, 2013.

[34] S. M. El-Bahy, D. A. Fadel, Z. M. El-Bahy, and A. M. Metwally, "Rapid and highly efficient cesium removal by newly synthesized carbomer encapsulated potassium copper hexacyanoferrate composite," *Journal of Environmental Chemical Engineering*, vol. 6, no. 2, pp. 1875–1885, 2018.

[35] S. Q. Chen, X. N. Yang, Z. Wang et al., "Prussian blue analogs-based layered double hydroxides for highly efficient Cs plus removal from wastewater," *Journal of Hazardous Materials*, vol. 410, Article ID 124608, 2020.

[36] B. Hu, B. Fugetsu, H. Yu, and Y. Abe, "Prussian blue caged in spongiform adsorbents using diatomite and carbon nanotubes for elimination of cesium," *Journal of Hazardous Materials*, vol. 217-218, pp. 85–91, 2012.

[37] Y. Han, A. A. Boateng, P. X. Qi, I. M. Lima, and J. Chang, "Heavy metal and phenol adsorptive properties of biochars from pyrolyzed switchgrass and woody biomass in correlation with surface properties," *Journal of Environmental Management*, vol. 118, pp. 196–204, 2013.

[38] F. Shiba, U. Mameuda, S. Tatejima, and Y. Okawa, "Synthesis of uniform Prussian blue nanoparticles by a polyol process using a polyethylene glycol aqueous solution," *RSC Advances*, vol. 9, no. 59, pp. 34589–34594, 2019.

[39] C. Loos-Neskovic, M. Fedoroff, and E. Garnier, "Zinc and nickel ferrocyanides: preparation, composition and structure," *Talanta*, vol. 31, no. 12, pp. 1133–1147, 1984.

[40] J. Liang, C. H. Li, and D. R. Talham, "Growth mechanisms of mesoscale Prussian blue analogue particles in modifier-free synthesis," *Crystal Growth & Design*, vol. 20, no. 4, pp. 2713–2720, 2020.

[41] H. Ming, S. Furukawa, R. Ohtani, H. Sukegawa, and Y. Yamauchi, "Synthesis of prussian blue nanoparticles with a hollow interior by controlled chemical etching," *Angewandte Chemie International Edition*, vol. 51, pp. 984–988, 2012.

[42] N. L. Torad, M. Hu, M. Imura, M. Naito, and Y. Yamauchi, "Large Cs adsorption capability of nanostructured Prussian blue particles with high accessible surface areas," *Journal of Materials Chemistry*, vol. 22, no. 35, pp. 18261–18267, 2012.

[43] F.-X. Bu, M. Hu, W. Zhang et al., "Three-dimensional hierarchical Prussian blue composed of ultrathin nanosheets: enhanced hetero-catalytic and adsorption properties," *Chemical Communications*, vol. 51, no. 99, pp. 17568–17571, 2015.

[44] E. Targholi, M. S. Rahmanifar, and S. M Mousavi-Khoshdel, "Facile synthesis of copper hexacyanoferrate/graphene nanocomposite for electrochemical energy storage," *Organometallic Chemistry*, vol. 32, p. 4615, 2018.

[45] J. Jang and D. S. Lee, "Magnetic Prussian blue nanocomposites for effective cesium removal from aqueous solution," *Industrial & Engineering Chemistry Research*, vol. 55, no. 13, pp. 3852–3860, 2016.

[46] S. Naeimi and H. Faghihian, "Performance of novel adsorbent prepared by magnetic metal-organic framework (MOF) modified by potassium nickel hexacyanoferrate for removal of Cs^+ from aqueous solution," *Separation and Purification Technology*, vol. 175, pp. 255–265, 2017.

[47] Y. Kim, Y. K. Kim, S. Kim, D. Harbottle, and J. W. Lee, "Nanostructured potassium copper hexacyanoferrate-cellulose hydrogel for selective and rapid cesium adsorption," *Chemical Engineering Journal*, vol. 313, pp. 1042–1050, 2017.

[48] H.-M. Yang, C. W. Park, I. Kim, and I.-H. Yoon, "Hollow flower-like titanium ferrocyanide structure for the highly efficient removal of radioactive cesium from water," *Chemical Engineering Journal*, vol. 392, Article ID 123713, 2020.